

# A stable corridor for toroidal plasma compression

Dylan Brennan,<sup>1</sup> Aaron Froese,<sup>2</sup> Meritt Reynolds,<sup>2</sup> Sandra Barsky,<sup>2</sup>  
Alex Wen,<sup>3</sup> Zhirui Wang,<sup>1</sup> Michael Delage,<sup>2</sup> and Michel Laberge<sup>2</sup>

<sup>1</sup>*Plasma Physics Laboratory, Princeton University, Princeton, NJ, USA*

<sup>2</sup>*General Fusion Inc., Burnaby, British Columbia, Canada*

<sup>3</sup>*University of British Columbia, Vancouver, British Columbia, Canada*

A toroidal plasma compressed by a collapsing flux conserver is analyzed to reveal stable scenarios of operation to high compression ratios. The resistive and ideal MHD stability is calculated in full toroidal geometry, using the asymptotic matching method in realistic conditions, and comparing with nonlinear simulations. The near edge current profile, controlled by toroidal field ramping during compression, is shown to be critical to stability due to coupling between poloidal components of the least stable mode. The extension of a length of shaft on axis is also found to be critical at high compression, as the resulting good curvature region in magnetic field stabilizes pressure driven modes that would otherwise be unstable. This work extends from previous studies, which initially showed the existence of a stable scenario, to include findings of more extensive stable zones, detailed effects of geometry, and nonlinear simulations of the instabilities. The nonlinear simulations of the compression are consistent with the linear analyses, confirming both the conservation and stability properties.

## I. INTRODUCTION

There has recently been a renewed interest in Magnetized Target Fusion (MTF) as a practical fusion concept. Perhaps the most promising of these experiments proposes to use toroidal plasma targets that are heated via compression to fusion conditions. The concept of using compression for the heating of plasmas dates back decades [1]. Recently, experiments at General Fusion have explored the viability of this concept [2], with compression of a spherical tokamak proposed for future large-scale devices [3]. An important requirement for successful MTF is that the plasma remain magnetohydrodynamically (MHD) stable during the compression. However, there are a number of compression effects that may cause the plasma to become unstable. These include the change of current profile due to evolution of the flux conserver geometry and the increase of the plasma  $\beta \equiv 2\mu_0 P/B^2$  ( $\beta$  is a measure of the thermal to magnetic energy density ratio). In order to properly design and successfully operate an experiment demonstrating the attainment of fusion conditions in MTF it is necessary to understand the plasma stability for the entire evolution of realistic geometric compression scenarios.

The heating of tokamak plasmas via magnetic compression has been studied experimentally on several conventional tokamaks, including the ATC experiment [4–6], TUMAN-3M [7], TOSCA [8], TFTR [9, 10] and JET [11, 12]. In particular, the ATC experiment was designed specifically for this purpose, producing significant compression ratios, and successfully demonstrating much of the basic concept. However, results from those experiments indicated the onset of resistive MHD instabilities, leading to disruptions and preventing access to the high confinement regimes. Some of the earliest seminal work into the theory of the MHD tearing mode [13–15]

emerged contemporaneously. While ideal MHD instabilities tend to grow rapidly irrespective of the resistivity, resistive MHD instabilities can grow more slowly, due to magnetic reconnection (i.e. tearing) occurring at resonant surfaces. Nevertheless, both can be disruptive given time to grow, and must be avoided. The stability of these modes depends on the detailed structure of the underlying equilibrium, and subtle physics effects in the plasma, such that computing it is not a trivial matter even today. While reduced theoretical analyses provided some insight at the time of the ATC experiments, the computational tools to accurately compute the stability had not yet been developed. The design of a controlled compression experiment that avoided these instabilities was evidently elusive.

The renewed interest in compression of tokamak plasmas is motivated by the many advantages of pulsed operation detailed in Ref. [3]. A prime advantage is that with the robust magnetic surfaces possible in toroidal geometry the energy and particle confinement times can be longer than mechanically achievable compression times making it possible to obtain fusion net gain (at the system level) before the plasma is extinguished by interaction with the wall. This, of course, requires the magnetic configuration to be one that remains stable during compression.

In Ref. [16], we presented an initial stability analysis that indicates a resistive MHD stable scenario of compression exists given carefully chosen plasma profiles and shaping. The study presented results of ideal and resistive MHD stability analyses of compression scenarios using realistic constraints to compute the equilibrium states. Toroidal equilibria produced with the CORSICA code [17] are analyzed with the DCON code [18]. The physics constraints, geometric structures, and magnetic equilibrium structure are designed to accurately capture

those of a proposed experimental MTF device with advantageous stability properties. The main results were presented in a parameter space of safety factor  $q_0$  vs compression ratio  $C = R_0/R$ , where  $R$  is the outboard midplane radius of the device, and  $R_0$  is the initial  $R$  before compression. In this space a stable “corridor” was found where a trajectory of a compressed experiment would narrowly avoid all computed instabilities. Control of the near edge current profile was found to be critical to the overall stability. Also, a nonlinear axisymmetric simulation is presented which indicates the degree of conservation and validity of the constraints used in the study. The results indicate that stable MHD pathways exist to high compression, affording insights that will be critical to the design and operation of any successful MTF device.

The main goal of the present work is to expand on the previous results, showing further stabilizing effects of edge current and geometry, and confirming the central result with nonlinear simulation. The resulting scenario has a wide stable corridor that is more experimentally viable than that of Ref. [16]. In addition, the stabilizing effect of the extent of a length of shaft on the geometric axis is shown to be critical to the stability at high compression, through comparison of two cases with and without the extension of shaft. Finally, new nonlinear simulations are presented using the VAC code [19], including non-axisymmetric instabilities, where it is found that an  $n = 2$  mode is unstable when the simulation is run in a parameter regime where linear theory indicates it should be. The simulations likewise remain stable in the stable corridor. These results provide further insight into the potential for compression and heating of tokamak plasmas while avoiding MHD instabilities.

The paper is organized as follows. In Sec. II we review the basics of compression, and its effects on confinement and the scaling of equilibrium quantities, while in Sec. III we review the constraints imposed to calculate equilibria in this study. In Sec. IV the results of stability analyses are presented, including the effects of near edge current profile changes and geometric changes to the confinement region. In Sec. V nonlinear MHD simulations of the compression are presented which indicate that the mode stability is consistent with the linear calculations. In Sec. VI the overall results are discussed, including a discussion of how the experiment could avoid the instabilities and remain stable.

## II. THE EFFECT OF COMPRESSION

A more extensive discussion of the compression physics appears in Ref. [16], while here we briefly review the main points. The basis of magnetic compression is in Alfvén’s frozen-in theorem. Magnetized collisionless plasma moves together with the magnetic flux [20] and so compression of magnetic flux also compresses the plasma.

In a plasma with nested flux surfaces the safety factor  $q$ , which measures how helical the field is as it winds through the torus, is connected to magnetic flux through  $q = d\Phi/d\Psi$ , where  $\Phi$  and  $\Psi$  are the toroidal and poloidal magnetic flux of the surface [21]. Therefore the  $q$ -profile is conserved during compression. Neglecting transport losses and assuming shock-free compression, the entropy profile  $S(\psi)$  of the plasma is also conserved during compression, while the temperature increases as described by thermodynamics.

Because the compression is slow compared to ion motion (i.e., adiabatic in the mechanical sense) but fast compared to the cross-field transport of magnetic flux, particles, and heat (i.e., adiabatic in the thermodynamic sense), we can model the effects of compression without loss of magnetic flux, magnetic helicity, thermal energy, or particles, or change of entropy, to a good approximation. The magnetic compression experiments described above have exhibited this “adiabatic compression” to varying extents [4–11].

Scaling laws for adiabatic magnetic compression of a tokamak plasma of major radius  $R$  and minor radius  $a$  were first given by Furth and Yoshikawa [22]. These laws are based on holding  $a^2 B_t$  fixed due to the toroidal flux conservation, holding  $a B_t / R B_p$  fixed due to conservation of  $q$ , and holding  $T/n^{2/3}$  fixed assuming thermally adiabatic compression. Some of the resulting geometrical scalings are

$$\begin{aligned} T &\propto a^{-4/3} R^{-2/3} \\ I_t &\propto R^{-1} \\ \beta_N &\propto a^{-1/3} R^{-2/3}, \end{aligned} \quad (1)$$

where  $I_t$  is the toroidal current and  $\beta_N \equiv a B_t / I_t$  is the Troyon factor that indicates how close the plasma is to major destabilizing MHD activity. The experiment should exhibit this scaling in equilibrium quantities along its trajectory of constant  $q$  if the geometry is compressed in such a way as to be well described by  $a$  and  $R$  variation.

## III. EQUILIBRIUM CONSTRAINTS DURING COMPRESSION

For this study, Fig. 1 represents a proposed MTF machine, simplified for the purpose of calculation. In this experiment a shell of liquid lithium mechanically compresses the plasma from the outboard direction. The magnetized plasma with closed flux surfaces is confined by currents induced in the surrounding liquid metal shell and through the shaft, which conserve the magnetic flux. The fields thus scale in much the same manner as in the magnetic compression experiments, albeit mechanically compressed.

In Fig. 1, the outboard midplane radius of the flux conserver starts at  $R_{fc}(t = 0) = 1.5$  m. The radial com-

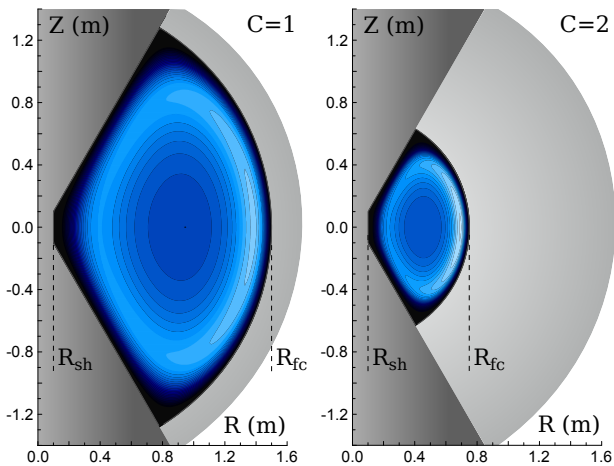


FIG. 1. CORSICA equilibria showing compression of plasma by a converging liquid metal shell. Contours indicate plasma current intensity,  $\mathbf{J} \cdot \mathbf{B}/B^2$ . The solid metal is dark gray and liquid metal is light gray.

pression ratio is defined as  $C \equiv R_{fc}(t=0)/R_{fc}(t)$ . The central shaft of the device is fixed at radius  $R_{sh}$ . For  $R_{sh}/R_{fc} \ll 1$  and given a nearly spherical compression, the initial geometric evolution will be nearly self-similar, making  $a, R \propto R_{fc}$  and  $T \propto 1/R^2$  in the above scalings. However, at high compression, as  $R_{fc}(t)$  approaches  $R_{sh}$  and the aspect ratio  $R/a$  changes, the scalings will follow Eq. 1. There will also be other geometric effects (e.g., change of elongation) that will cause the scaling to deviate from that of Furth and Yoshikawa, which is clearly observed in computations.

We use an approach based on stability analysis of Grad-Shafranov equilibrium states. The equilibrium state is relevant because the Alfvén time in the experiment is always much shorter than the compression time. Thus, the experiment is in quasi-equilibrium throughout the compression. Starting from an initial plasma equilibrium in uncompressed geometry, subsequent equilibria in compressed geometries are generated using CORSICA with pressure given by the entropy constraint, while toroidal field and current are given by the constraint on  $q$ .

Fig. 2 (a) shows an initial profile of pressure and  $q$  as a function of normalized poloidal magnetic flux for a typical shaft current of 1.9 MA and a plasma current of 1.55 MA. As the shaft current is varied the plasma current and pressure are held fixed and the  $q$  profile varies accordingly. The core of the two dimensional cross section shown in Fig. 1 is at ( $\bar{\psi} = 0$ ), while ( $\bar{\psi} = 1$ ) is at the outer boundary of the plasma. The  $q$  profile is reversed on axis with an off-axis minimum at low shaft current ( $\approx 500$  kA), but is monotonic at high shaft current ( $\approx 2$  MA). The  $q$  profile shown in Fig. 2 (a) is monotonic at 1.9 MA.

The equilibria are limited on the outboard midplane,

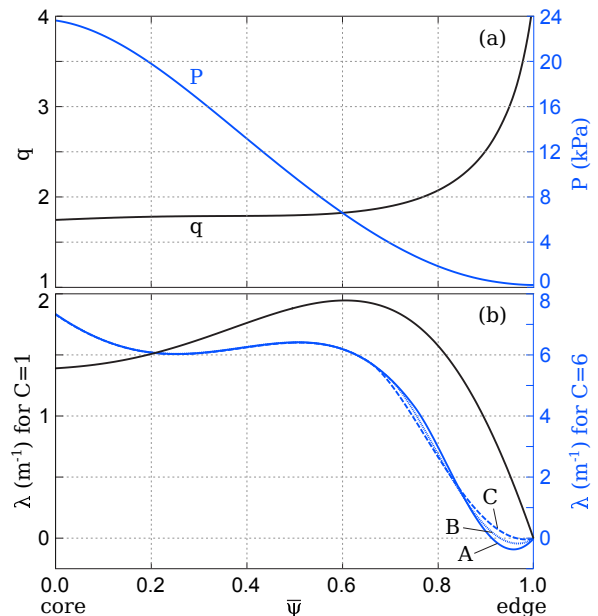


FIG. 2. Profiles versus normalized poloidal flux of safety factor  $q$  in black and pressure in blue (a) of an uncompressed equilibrium, and  $\lambda \equiv dF/d\psi$  (b) with no compression  $C = 1$  in black and with  $C = 6$  in blue. The initial shaft current is 1.9 MA. The edge region develops a reversed skin current to maintain the  $q$  profile. Three  $\lambda$  profiles at compression  $C = 6$  have varying edge structure in cases A, B and C. The structure of the edge  $\lambda$  can be varied in experiment by controlling the shaft current during compression.

with a thin vacuum region of 5% of the major radius throughout the compression. This is intended to model experimental observations of this region during compression, where a cold plasma is observed surrounding the core plasma. This is analogous to the vacuum region modeling in conventional tokamak stability analyses.

The shaft is solid metal in this model to simplify its treatment during compression. In a fusion power plant the high heat flux and pressure experienced by the shaft would likely make a solid shaft impracticable. Instead, a liquid metal shaft could be used. A realistic model would need to include heating and compressible MHD flow of the liquid metal for both the liner and the shaft. However, the effect on plasma geometry, and hence the stability analysis, is expected to be small in the trajectory leading up to fusion conditions.

The shape of the pressure and  $q$  profiles are largely fixed throughout compression, but the  $\lambda$  profile is not ( $\lambda \equiv dF/d\psi$  with  $F = rB_\phi$ ; for low plasma beta the  $\lambda$  profile is related to the parallel current density profile through  $\lambda \approx \mu_0 \mathbf{J} \cdot \mathbf{B}/B^2$ ). In Fig. 2(b) the  $\lambda$  profiles of equilibria at initial ( $C = 1$ ) and high compression ( $C = 6$ ) are shown. An initial  $\lambda$  profile that peaks outside the core region in mid-radius proved both to be advantageous in terms of overall stability during compression and experimentally viable as an initial state. The core

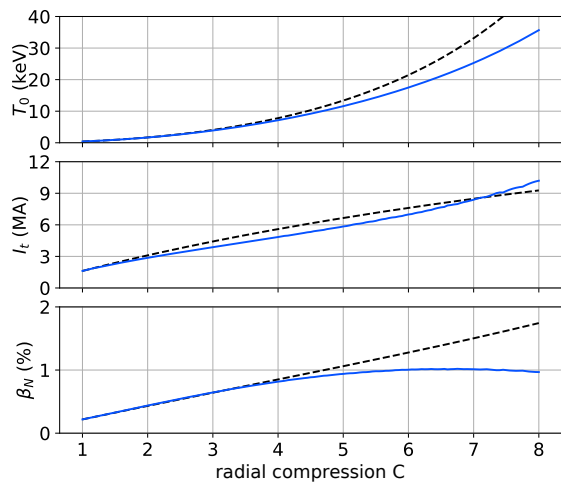


FIG. 3. Temperature at the magnetic axis, plasma current, and normalized beta taken along compression trajectory (a horizontal line in Fig. 4 with  $q_0 \approx 1.76$ ). Dashed lines show the scalings described by Eqs. 1.

region of the  $\lambda$  profile peaks slightly during compression. However, at high compression  $\lambda$  reverses near the edge of the plasma, effectively forming a skin current, due to the  $q$  profile constraint and changing geometry. This reversed current can be induced in both experiment and resistive MHD simulations. Note the plasma in the edge is cooler and therefore more resistive, so fine scale edge current structure tends to be dissipated. The series of Grad-Shafranov equilibrium states generated assuming conservation of  $q$  does not account for this effect, being a solution to the ideal MHD equations that does not include resistivity. To explore the effect of varying the edge structure in the current profile, series A, B and C were generated with varying degrees of smoothing applied to mimic the effect of resistivity. The  $q$  profile is weakly affected by these variations. However, the depth and amplitude of the skin current was found to be critical to the stability of the plasma, in particular because gradients in  $\lambda$  across resonant  $q$  surfaces tends to be destabilizing [15].

Fig. 3 shows  $\beta_N$ , plasma current  $I_t$ , and temperature  $T$  of an equilibrium with  $q_0 = 1.76$  as a function of  $C$ . Despite the soaring density and temperature, the  $\beta_N$  of the equilibria remain reasonable, giving us some hope that we can maintain a stable plasma throughout compression. The scaling relations in Eqs. 1 are plotted (dashed lines) for comparison; initially the computed quantities scale as Eqs. 1, but differ at high  $C$  as the elongation increases and the volumetric compression rate decreases.

During compression, the natural increase of shaft current induced by the conservation of toroidal flux can be supplemented by an external applied voltage to control its rate of increase. Any such action will naturally induce a poloidal skin current in the plasma edge which will have

a parallel component. Thus, to some extent, it is feasible to control the structure of  $\lambda$  near the edge during compression. Therefore, for this study, we varied the edge gradient of  $\lambda(\bar{\psi}, C)$  to study the effect on stability. The  $C = 6$  profile shown in Fig. 2(b) is a case found to be both sufficiently stable and consistent with experimental conditions.

Fig. 2(b) shows three profiles of  $\lambda$  at the same compression ratio of  $C = 6$  and the same initial conditions before compression with  $q_0 = 1.75$ , but with different gradient in the  $\lambda$  profile near the edge during compression. Though the variation in  $\lambda$  appears moderate, the stability can be strongly affected, as shown below and in Ref. [16].

#### IV. STABILITY CALCULATIONS

We analyze the equilibria calculated from CORSICA with Resistive DCON (RDCON) [23]. RDCON calculates the ideal MHD perturbed potential energy,  $\delta W$ , and the resistive MHD stability based on the method of matched asymptotic expansions in full toroidal geometry, where the plasma is partitioned into the ideal outer region and resistive inner region around each rational  $q$  surface. The zero-frequency ideal MHD equations, governing the outer region, are cast as a Euler-Lagrange equation [24] for a given toroidal number  $n$ . The poloidal mode structure is represented as a spectrum of components with wave numbers  $m$ . Both the ideal and resistive MHD stability of a single  $n$  mode are described by the global eigenmode solution which couples all  $m$  components together for a single  $n$ .

In general, the equilibrium states we seek must be both locally and globally stable. Perhaps the most fundamental stability consideration is given by the local resistive interchange stability, which is defined by the energetic favorability of the swapping of neighboring regions of plasma field lines. The local resistive interchange parameter  $D_R$  is a measure of this instability and must remain negative [14]. In ideal MHD, the interchange can occur without breaking field lines, giving a closely related stability criterion represented by  $D_I$  which must also remain negative. Both quantities depend on the local equilibrium characteristics, such as pressure gradient and magnetic shear. For the equilibrium and stability profiles and geometries presented here, both quantities remain negative at all surfaces, which leaves the global stability to be considered.

Both  $D_I$  and  $D_R$  are calculated as flux averaged quantities around the poloidal direction, are functions of minor radius of the plasma, and appear as driving terms in the global stability calculation [14, 25, 26], representing the local contributions to the global stability. In the calculation, the field line curvature contributes to the local, and thereby global stability [27].

The stability of the global solution during compression bears some analogy to the Kadomtsev criterion in cylindrical Z-pinch experiments [28], where the pressure gradient and magnetic field shear analogously drive global instabilities. However, the equilibria here remain tokamak-like throughout the compression. In general, tokamak configurations tend to have favorable (stabilizing) field line curvature on the inboard or high field side of the poloidal cross section, and unfavorable (destabilizing) curvature on the outboard or low field side. It is for this reason that modern conventional tokamaks, such as DIII-D [29] and ITER [30], are designed in D-shaped cross sections, placing more poloidal extent in the good curvature inboard side of the cross section. The stabilizing influence of the inboard good curvature region is enhanced at low aspect ratio, and it is in part for this reason that spherical tokamaks such as NSTX-U [31] and MAST [32], also with D-shaped cross sections, exhibit such high stability limits in  $\beta$ . In the results presented here, it is for this same reason that exposing a length of shaft is found to be stabilizing to the highly compressed states, as discussed below, by making them more D-shaped and extending the good curvature region.

At each surface in the plasma where the safety factor matches the ratio of integer poloidal and toroidal wave numbers,  $q = m/n$ , a resonance occurs. Such surfaces will form resonant layers in the plasma, with highly localized currents sensitive to the resistivity of the plasma.

If the equilibrium is ideal stable, the free energy available to a resistive mode is described by the local stability index  $\Delta'$ , calculated from the resonant response at each layer. The assembly of all rational surfaces of a given toroidal wave number  $n$  then produces the matrix of non-ideal stability indices, e.g., the  $\Delta'$  matrix.

Each layer response is then calculated including resistivity based on the Glasser, Greene and Johnson model [14], to form a diagonal matrix of layer response functions. In short, the eigenvalue problem for the growth rate can be expressed as finding the root of a determinant  $|D' - D(Q)| = 0$  where  $D'$  is the matrix of stability indices calculated from the global mode structure,  $D(Q)$  is a diagonal matrix of layer responses at each rational surface, and  $Q$  is the complex eigenvalue, the real part of which is the growth or decay rate of the mode. The detailed description of the whole process in RDCON can be found in [23].

### A. The stable corridor

Given an initial set of equilibria with varying shaft current, at fixed plasma current and pressure, we then define a two dimensional space of equilibria by compressing each of these initial states and employing the physics constraints discussed to determine each equilibrium and test its stability. Fig. 4 shows the equilibrium and stabil-

ity results of this analysis for three different constraints on the sharpness of the edge current profile, as shown in Fig. 2(b). Cases A, B and C in Fig. 2(b) refer to Figs. 4(a), (b) and (c) respectively. The left hand axes of Fig. 4 show the  $q_0$ , the safety factor at the magnetic axis. The equilibria are generated in equal increments of  $1/R$ , making the high compression region highly resolved in compression steps. The shaft current during compression is shown in magenta contours. The plasma temperature, and points on the safety factor profile:  $q_{\min}$ , and  $q_{95}$ , appear as dashed lines. The plasma  $\beta$  increases with  $C$  despite the increasing toroidal field, reaching values of  $\sim 0.3$  at low shaft current and  $\sim 0.15$  at high shaft current for  $C = 8$  (not shown). Horizontal paths through this space represent adiabatic compression trajectories, such as Fig. 3. Note that realistic compression trajectories that include losses will deviate from a horizontal line in this space, especially as the edge current changes. However, these deviations are generally expected to be small, as is shown below through MHD simulation.

In Fig. 4 the growth rate for the  $n = 1$  mode is plotted as colored contours. Ideal instability is shown in red. The ideally unstable region for  $q_0 \lesssim 1.25$  is primarily due to the  $m/n = 1/1$  mode; but when  $q_{\min} > 1$ , the non-resonant  $1/1$  component couples into the higher  $m > 1$ ,  $n = 1$  components to drive instability. We note that other profile and geometric structures explored were found to be susceptible to ideal pressure driven instabilities at high  $C$ , highlighting the advantageous properties of the profiles and geometric structure used here. An example of a more unstable configuration is discussed below. A second ideal unstable region is found just below  $q_{\min} = 2$ , where the  $q = 2$  surface approaches the axis, and the  $q = 4$  surface enters the plasma at the edge, intermittently unstable depending subtly on the details of the equilibrium, hence the dashed line. Though this mode is expected to be rather benign to the confinement, the experiment would avoid this instability.

Fig. 4 shows that a strongly resistive MHD unstable zone over a wide range of  $C$ , just above the dotted  $q_{95} = 2$  line for  $q_0 \approx 1.4$ , for all three cases. This is a  $2/1$  dominant mode and would likely be highly disruptive in experiment. As the initial shaft current or  $q_0$  is increased, however, this mode becomes stabilized and a stable channel appears to high compression near  $q_0 \approx 1.75$ . A second unstable region appears above  $q_0 \approx 1.85$  for Case A, and above  $q_0 \approx 1.95$  for Case C, indicating that as the edge current is flattened, the corridor widens significantly. This upper unstable region is a  $m/n = 3/1$  dominant mode, with coupling between the  $q = 2$  and  $q = 3$  resonant surfaces on its lower end, while above  $q_{\min} = 2$  the non-resonant  $m = 2$  component plays a role, and coupling to the  $q = 4$  surface becomes more important.

The three stability results shown in Fig. 4(a)-(c) correspond to the varying edge current constraint, changing the structure of the edge current as shown in Fig. 2(b).

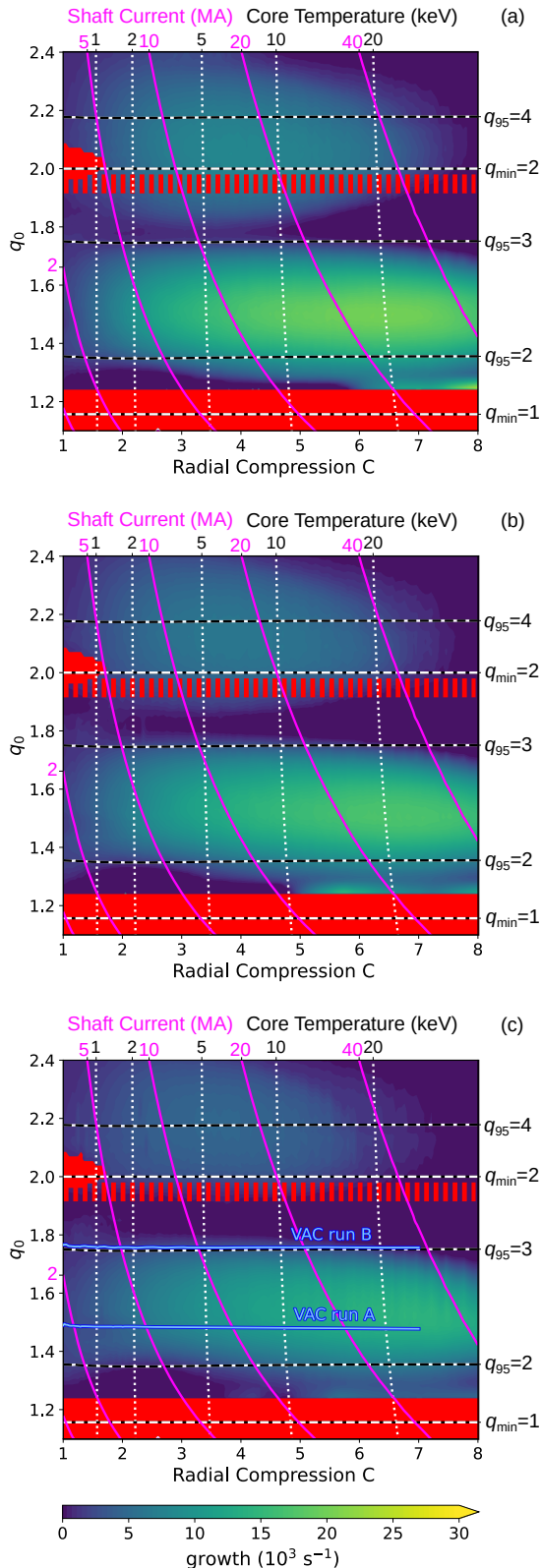


FIG. 4. Stability results from an RDCON analysis of  $n=1$  modes as the edge current structure is changed. Ideal instability is shown in red, resistive instability in green/yellow, and stability in dark blue. Dotted white contours indicate plasma core temperature in keV. Safety factor values  $q_{\min}$  and  $q_{95}$  are indicated by black and white dashed contours. Magenta contours show shaft current in MA.

As the edge current gradient is reduced, the stable corridor is widened. The structure of  $\lambda$  does not vary greatly in these figures as a function of  $q_0$ , instead it mainly varies in amplitude with  $q_0$ . The main effect on stability in varying initial shaft current and  $q_0$  is to change the radii of the rational surfaces and the coupling between mode components. The  $q$  profiles tend to be flattened or slightly reversed in the core, as shown in Fig. 2, with rational surfaces near the edge. With lower gradients in  $\lambda$  near the edge, the stable corridor widens between where the 2/1 dominant mode and the 3/1 dominant mode are unstable, as seen in Fig. 4(c).

Fig. 4 portrays results for three cases with moderate edge current. Larger edge current and, in particular, gradients in  $\lambda$  across surfaces enhance the coupling between the  $q = 2$  and  $q = 3$  surfaces, destabilizing the modes and closing off the stable corridor. Ref. [16] details one such case.

Two trajectories obtained by using the VAC code [19] to evolve the resistive MHD equations in time-dependent geometry are superposed on the RDCON results in Fig. 4(c). In these 3D simulations the resistive  $n \geq 1$  stability of the plasma is included, as discussed below. However, even just the axisymmetric profile evolution and conservation during compression are informative. The shaft current and pressure and  $\lambda$  profiles from the uncompressed equilibrium represented in Fig. 4 are used as initial conditions for the VAC simulations. We note that the nearly horizontal trajectory confirms that  $q$  is reasonably constant during the 3 ms long compression in a realistic simulation. The nonlinear stability of these simulations is discussed in detail below in Sec. V.

## B. Stability Dependence on Shape and Profiles

In Fig. 5 two series of boundary configurations are shown over a compression factor of  $C = 8$ . Both outer boundaries have the same angle off the central axis of  $\pi/6$ . In the first the boundary has no flat region along the shaft, while in the second the boundary has a 20 cm section that is flat along the shaft. This central section will change the stability of the compressed equilibria, while having little effect on the initial equilibria or the experimental start up. The results shown in Fig. 4 use the boundary configuration in Fig. 5(b), including the flat section on the shaft.

The stability of the equilibria for both of these series of shapes, for  $n = 1, 2$  and  $3$ , is shown in Figs. 6 and 7. The equilibria for both start from  $T = 400$  eV and  $n = 5 \times 10^{19} \text{ m}^{-3}$ , which is typical of the temperature and density of the Ohmic heated plasmas before compression. And, the profiles are initially identical. Note that Fig. 7(a) for  $n = 1$  repeats from Fig. 4(c) in comparing the effect of  $\lambda$  near the edge.

At high compression, the longer shaft region provides

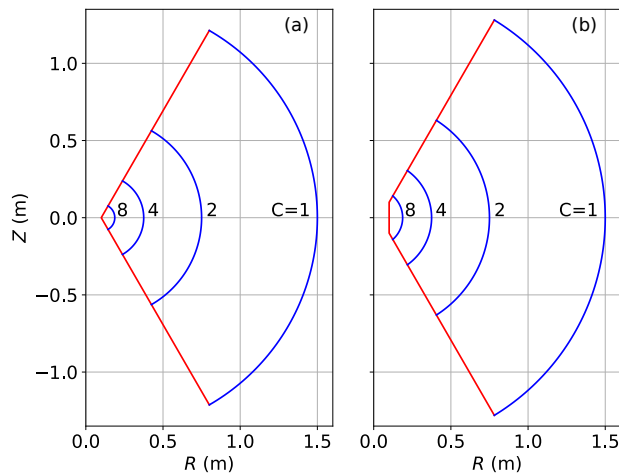


FIG. 5. The boundary shapes of two series of equilibria varying the length of the central shaft. This affects the stability most at high compression.

a significantly larger poloidal region of good magnetic curvature, causing a stabilizing effect. This effect can be seen by comparing the right sides (i.e.  $C > 5$ ) of Fig. 6 with right sides of Fig. 7. The left side of these figures,  $C < 4$ , are similar for both shapes, as early in the compression sequence, the relatively small difference in the shaft length has little effect. Later in the sequence, at high compression, the case with no shaft length is increasingly more unstable with compression.

With no flat region along the central shaft, at higher compression  $C > 4$  unstable regions extend to lower compression as shown in Fig. 6. The vertical and tilt modes are held stable due to the 30 degree walls at top and bottom. However, with less good curvature, kink and tearing modes, with a ballooning component, are driven unstable. Following any horizontal trajectory from left to right in Fig. 6 would eventually have a tearing mode unstable with increasing growth rate, with several trajectories indicating entry into an ideal unstable region. The ballooning component to the mode is evidenced as the higher  $n$  is more unstable for the lower  $q_0$  cases, noting that Fig. 6(c), with  $n = 3$  is ideal unstable at lower compression and over a wider region than Fig.6(a) with  $n = 1$ . Also, the ideal unstable zones are increasing in width at higher compression. Clearly there is no fully stable pathway with no shaft length exposed. With the shaft exposed, the configuration is stable for all  $n = 1, 2$  and  $3$ , in a range of  $1.75 < q_0 < 1.9$ , for all compression  $C$ , as shown in Fig. 7. And, the  $n = 2$  and  $3$  likewise remain stable as the good curvature region along the shaft stabilizes the mode.

## V. SIMULATIONS OF COMPRESSION

The linear stability of the configuration in Fig. 5(b), shown in Fig. 7, informs us about what to expect from a nonlinear MHD simulation of compression with these boundary shapes. Simulations with the VAC code [19] were conducted to test the prediction in Fig. 7, including the length of shaft in the geometry, starting with the same profiles on the left hand side of Fig. 7, and compressing the boundary while allowing the conservation in the MHD equations to manifest the plasma heating during compression.

The results from two simulations are presented in Fig. 8, one with  $q_0 = 1.5$  (run A) and the other with  $q_0 = 1.75$  (run B). The simulations include 32 toroidal planes to capture toroidal perturbations. From Fig. 7, in these simulations the resistive stability of the plasma should and does show a fast growing  $n = 2$  instability for the  $q_0 = 1.5$  case.

The compression in VAC is implemented by Strang splitting the operations of resistive MHD and of morphing the geometry along the sequence in Fig. 5(b). The shaft current, pressure and  $\lambda$  profiles from the uncompressed equilibrium represented in Fig. 2 are used as initial conditions for the VAC simulation. Resistive evolution is modeled assuming Spitzer resistivity with  $Z_{\text{eff}} = 1.5$ . Momentum transport is modeled using a uniform isotropic viscosity  $\mu \approx 7.5 \times 10^{-8}$  kg/m/s. This value is 10 times lower than the viscosity that stabilizes the plasma instability and approximates a realistic momentum transport in the simulation, while zero viscosity is assumed in the linear stability analysis. The magnetic Prandtl number in these cases is  $\text{Pr}_m \equiv \nu/\eta \approx \mathcal{O}(10)$  to  $\mathcal{O}(100)$ , where  $\nu = \mu/\rho$  is the viscous diffusion coefficient,  $\rho$  is the mass density, and  $\eta$  is the resistive diffusion coefficient. Classical perpendicular heat transport was used in the simulations as a physical approximation to the adiabatic compression assumption used throughout this paper. Extensive simulations from our previous work [16] indicate that  $q_0$  remains roughly constant during compression even for anomalous transport with  $\chi_e$  up to  $20 \text{ m}^2/\text{s}$  and  $\chi_i$  up to  $5 \text{ m}^2/\text{s}$ . Parallel heat transport was implemented using a non-Fourier (hyperbolic) method enabling physically realistic fast transport (the ratio of cross to parallel thermal conductivity is  $\mathcal{O}(10^{-10})$ ). To facilitate a numerically stable simulation the electron sound speed used in the parallel transport and the ion sound speed used in the MHD are artificially lowered by a factor of 10 and the Boris fix [33] is used with a reduced speed of light  $c' = 5 \times 10^5$  m/s. The boundary conditions imposed at the metal walls include zero flux diffusion, zero mass flux, and a low temperature. The thermal conduction to the cold wall results in a cold layer of plasma near the wall. A similar cold plasma layer is found in models of Z-pinch experiments [34]. Ini-

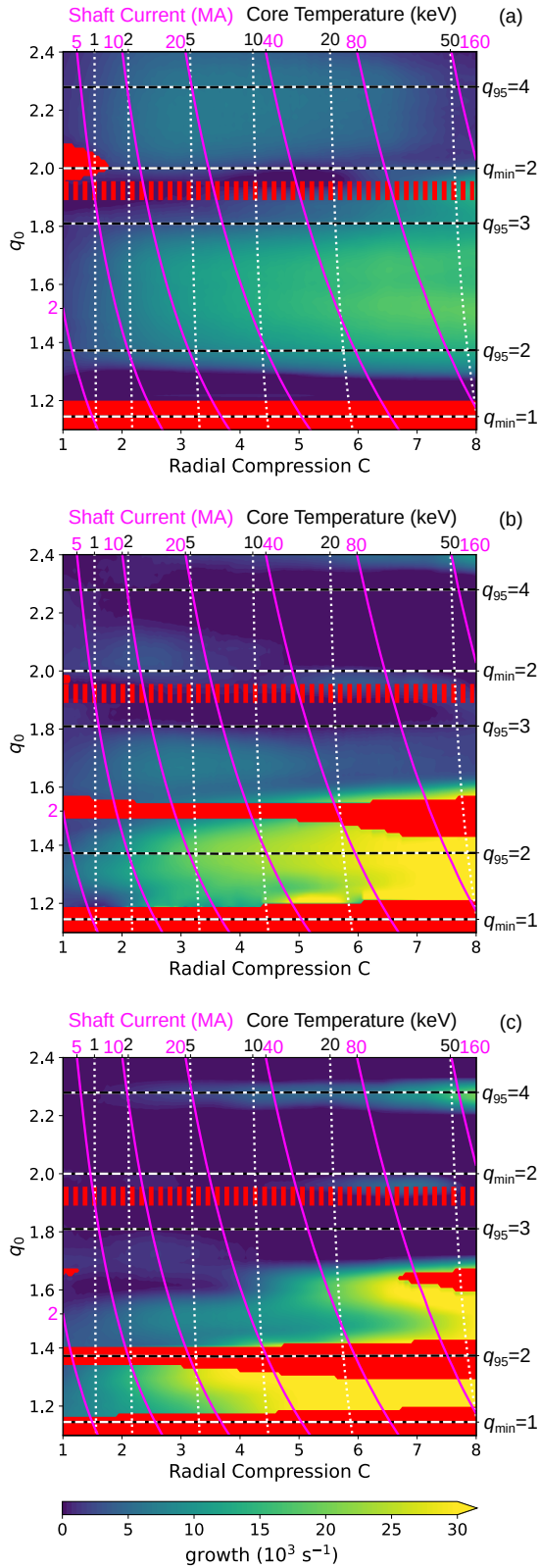


FIG. 6. The  $n = 1$  (a), 2 (b), and 3 (c) stability from RDCON of the boundary shapes in Fig. 5(a), with no length along the central shaft. Ideal unstable regions are red, while all other regions show resistive instability in green/yellow, and stable in dark blue.

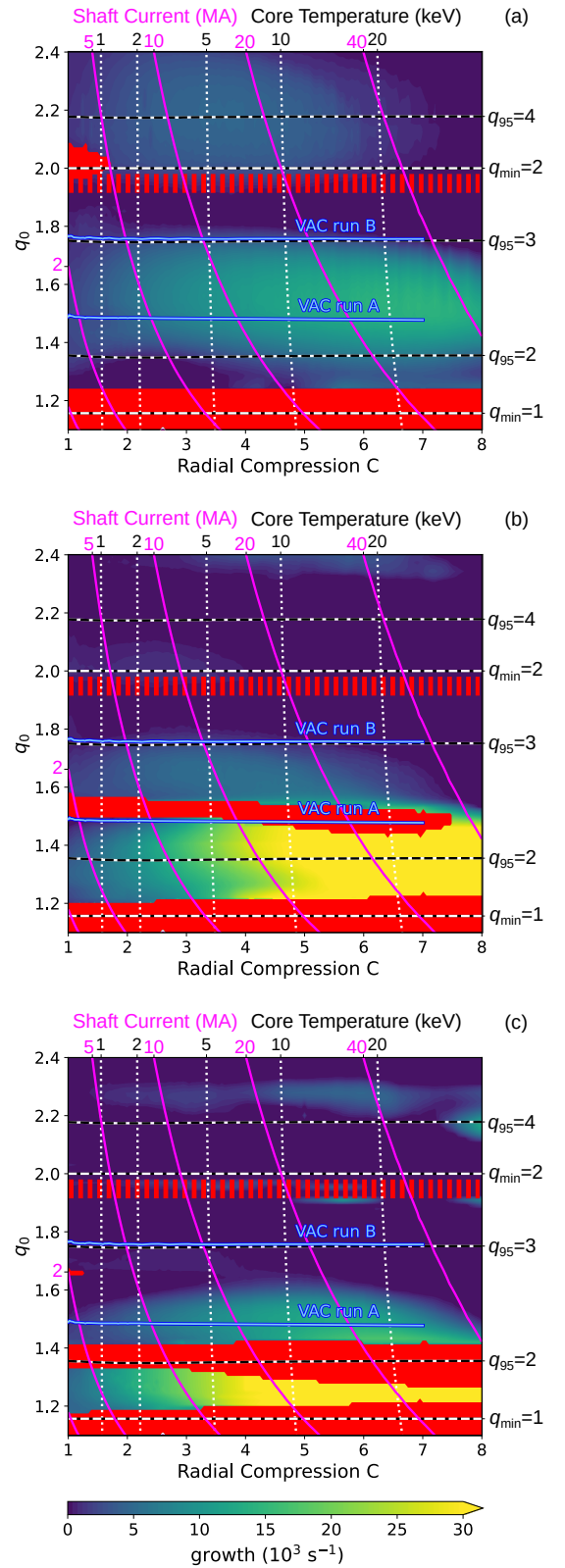


FIG. 7. The  $n = 1$  (a), 2 (b), and 3 (c) stability from RDCON of the boundary shapes in Fig. 5(b), with 20 cm along the central shaft. Ideal unstable regions are red, while all other regions show resistive instability in green/yellow, and stable in dark blue. Trajectories from two VAC MHD simulations are shown as blue lines.

tial ion density was uniform with  $n_i = 3 \times 10^{19} \text{ m}^{-3}$  and  $n_e = Z_{\text{eff}} n_i$ . Initial temperatures at the magnetic axis were  $T_e = T_i = 400 \text{ eV}$ , consistent with the linear calculations. More realistic transport modeling is planned for future work, in part to study the extent to which this would change both the equilibrium constraints and the stability. However, the present implementation both exhibits adiabatic-like confinement during compression and remains computationally tractable.

The VAC simulations exhibit a high degree of  $q$  conservation, which manifests as nearly horizontal trajectories in the figures. Realistic compression trajectories that include 3D effects and losses will naturally traverse the maps in a somewhat more complex way, especially as the edge current changes. However, deviations from a horizontal line are generally expected to be small.

The resulting perturbed magnetic fields were Fourier analyzed into a spectrum of toroidal components with wave numbers  $n$ , and the resulting energy in each of the first three non-axisymmetric components  $n = 1 - 3$  as a function of compression ratio  $R_0/R$  is shown in Fig. 8. The magnetic energies in Fig. 8 are normalized to the  $n = 0$  energy, which removes the effect of the increasing overall magnetic energy with compression and makes the stability of the modes in the simulations more intuitively accessible. The upper graph, for  $q = 1.5$ , shows that a mode with  $n = 2$  becomes unstable at radial compression ratio  $C = 3$ , and saturates relative to the background field. The lower graph, for  $q = 1.75$ , clearly indicates that no modes are unstable.

Note that the VAC trajectory shown in Fig. 7 indicates that although the  $n = 2$  mode should be most unstable in the simulation, which it is, there should also be slow growing  $n = 1$  and  $n = 3$  modes. Though the  $n = 1$  and  $n = 3$  energies do not drop off in Fig. 8(a) as they do in Fig. 8(b), the manifestation of the linear growth is not clearly separable from the nonlinear coupling due to the  $n = 2$  mode. More detailed study of the nonlinear MHD trajectories in the space of the linear results will continue, but this result supports a verification of the linear results, and shows how they manifest in nonlinear simulation and, under the right conditions, experiment.

## VI. DISCUSSION

The results shown here indicate that toroidal MTF compression experiments can be kept stable to ideal and resistive MHD instabilities through to high compression. Extensive MHD analyses with DCON were conducted, where it was found that including a small length of shaft allows for stability at high compression, while not affecting the early compression stages, which it is energetically favorable to compress self similarly. This stability comes through good curvature region along the shaft. The departure from self similar compression also serves

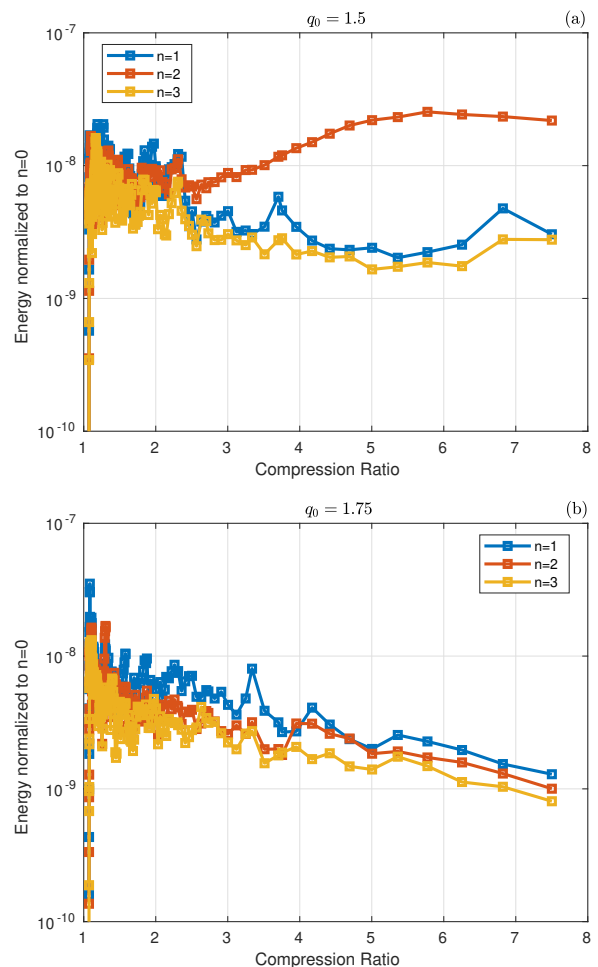


FIG. 8. Magnetic energies of modes 1-3 as calculated in VAC. The top graph (run A) has  $q = 1.5$ , and is in the unstable zone. The bottom (run B) has  $q = 1.75$ , and is in the stable zone.

to prevent higher  $\beta_N$  that would make it more difficult to maintain stability. The structure of the near edge current is also shown to be critical to the ideal and resistive stability. Extending from Ref. [16], a wider corridor of stability is found by nearly zeroing out the edge  $\lambda$  profile. The edge current can be controlled by the rate of ramping shaft current, and the slight adjustments necessary to maintain stability appear viable.

Nonlinear MHD simulations with the VAC code indicate that the linear instabilities are manifested in the nonlinear evolution. Specifically the  $n = 2$  instability was observed in simulations where it was the most unstable in the linear map. Also, a nonlinear simulation trajectory that passed through the stable corridor showed no instabilities through to high compression. Note that this trajectory (run B) passes just at the upper edge of the  $n = 1$  unstable region, with a very low but finite linear growth rate for part of the trajectory. It should be noted that the nonlinear simulations have dissipation, including

viscosity, which can modify the resonant layer response from the linear model employed, and change the profiles slightly from the equilibria calculated for the linear analyses, in particular near the edge. In strongly unstable regions, however, small variations such as these are not typically able to stabilize the mode, and the mode manifests in nonlinear simulation. Evidently the linear mode along the run B trajectory is not strong enough to manifest in the nonlinear simulation. In this sense, the linear results should be taken only as a guide for what to expect in nonlinear simulation and experiment, as more detailed physics models can change the stability, most readily in regions of near marginal stability.

An important physical effect not included in this analysis is that of diffusion of magnetic flux into the liquid metal wall. Due to resistivity of the liquid metal, the initially closed flux surfaces penetrate into the wall and become open flux. This loss of flux surfaces has the effect of shaving off the high edge  $q$ . There are also consequences for plasma-wall interaction. Current that was flowing on the surfaces as they are opened will decay rapidly; this may have the effect of inducing edge current on the remaining plasma. Plasma on the opened flux surfaces will be lost to the wall, resulting in an enhanced sputtering of wall material. The severity of this will depend on the initial current and density profiles which can perhaps be tailored to be little different from vacuum on the surfaces that will be lost. These effects are currently being investigated and will appear in a future publication.

A few other important physical effects not included in these results are resonant interaction with non-thermal or energetic particles, plasma rotation and two fluid effects. In all three cases, the equilibrium state and stability may be affected. Below we highlight a few key physics issues with each effect.

Once the plasma is compressed to tens of keV, a non-uniform source of alpha particle heating from fusion alphas is expected, an effect not taken into account in this work. This would be most pronounced at high compression, and after long enough for the ion distribution to collisionally form a slowing down distribution. While the equilibrium and stability may be affected here, the low compression and entry to the high compression regions will not. In that sense, this work is more focused on how to remain stable during compression than during the dwell time at maximum compression. We note that in the stable corridor, the energetic ion interaction should be stabilizing for the monotonic  $q$  profile [35], though this remains to be investigated.

For rotation, angular momentum conservation dictates that any initial rotation will increase with compression. While the differential rotation between surfaces is expected to have a stabilizing influence [36, 37], it is possible to drive rotational instabilities at high compression. Rotational effects are therefore currently being investigated. At high compression, the rotation can become

large enough that it must be taken into account in the equilibrium, where initial calculations indicate that the Mach numbers can reach  $M \gtrsim 0.1$ , but remain subsonic.

Last, the electron and ion temperatures can in general differ, and do in the VAC simulations, though a single fluid approach was used in the linear analyses presented here. We expect that two-fluid effects in the resonant layers will also change the linear stability to some degree, and may be necessary to better complement nonlinear simulations with VAC. Thus, these effects are also being investigated.

However, if the primary MHD instabilities described here are avoided, such experiments will likely be able to reach high compression ratios while remaining stable. It is only once high compression is reached that issues such as heat load and plasma wall interactions can be studied in detail experimentally.

- 
- [1] A. Robson, Report of NRL Progress, June 1973 (1973).
  - [2] A. Froese, S. Howard, V. Suponitsky, J. Zimmermann, M. Reynolds, S. Barsky, J. McCone, R. Ivanov, D. Parfeniuk, P. O'Shea, D. Richardson, M. Delage, and M. Laberge, in *19th Pacific Basin Nuclear Conference (PBNC 2014)* (Canadian Nuclear Society (CNS), 2014) p. 2151.
  - [3] M. Laberge, *Journal of Fusion Energy* **38**, 199 (2019).
  - [4] K. Bol *et al.*, PPPL Technical Report (1974), 10.2172/4203067, doi:10.2172/4203067.
  - [5] K. Bol *et al.*, *Phys. Rev. Lett.* **29**, 1495 (1972).
  - [6] K. Bol *et al.*, Fifth IAEA Conference Proceedings, Tokyo, Plasma Phys. and Controlled Nucl. Fusion **1**, 83 (1974).
  - [7] L. Askinazi *et al.*, *J. Plasma Fusion Res. SERIES* **4**, 224 (2001).
  - [8] D. Robinson, *Nuclear Fusion* **25**, 1101 (1985).
  - [9] G. Tait, M. Bell, and J. Bell, Plasma Phys. and Controlled Nucl. Fusion Research (Tenth IAEA Conference Proceedings, London, 1984) **1**, 141 (1985).
  - [10] D. J. Grove and D. M. Meade, *Nucl. Fusion* **25**, 1167 (1985).
  - [11] J. Wesson, "The science of JET" *JET-R(99)* **13** (1999).
  - [12] A. Tanga, JET Joint Undertaking Progress Report 1986, EUR 11113 EN (EUR-JET-PR4) , 211 (1987).
  - [13] B. Coppi, J. M. Greene, and J. L. Johnson, *Nucl. Fusion* **6**, 101 (1966).
  - [14] A. H. Glasser, J. M. Greene, and J. L. Johnson, *Phys. Fluids* **18**, 875 (1975).
  - [15] H. P. Furth, P. H. Rutherford, and H. Selberg, *The Physics of Fluids* **16**, 1054 (1973), <https://aip.scitation.org/doi/pdf/10.1063/1.1694467>.
  - [16] D. Brennan, A. Froese, M. Reynolds, S. Barsky, Z. Wang, M. Delage, and M. Laberge, *Nuclear Fusion* **60**, 046027 (2020).
  - [17] J. Crotinger *et al.*, LLNL Report **UCRL-ID-126284** (1997), 10.2172/522508.
  - [18] A. Glasser, *Physics of Plasmas* **23**, 072505 (2016).
  - [19] G. Tóth, *Astrophys. Lett. Commun.* **34**, 245 (1996).
  - [20] H. Alfvén, *Nature* **150**, 405 (1942); H. Alfvén, *Arkiv for Matematik, Astronomi och Fysik* **29**, 1 (1943).

- [21] A. H. Boozer, *Rev. Mod. Phys.* **76**, 1071 (2005).
- [22] H. P. Furth and S. Yoshikawa, *The Physics of Fluids* **13**, 2593 (1970), <https://aip.scitation.org/doi/pdf/10.1063/1.1692832>.
- [23] A. Glasser, Z. Wang, and J.-K. Park, *Physics of Plasmas* **23**, 112506 (2016).
- [24] A. H. Glasser, *Physics of Plasmas* **23**, 072505 (2016), <https://doi.org/10.1063/1.4958328>.
- [25] D. P. Brennan, A. D. Turnbull, M. S. Chu, R. J. La Haye, L. L. Lao, T. H. Osborne, and S. A. Galkin, *Physics of Plasmas* **14**, 056108 (2007), <https://doi.org/10.1063/1.2515224>.
- [26] S. E. Kruger, C. C. Hegna, and J. D. Callen, *Physics of Plasmas* **5**, 455 (1998), <https://doi.org/10.1063/1.872738>.
- [27] J. Freidberg, *Ideal MHD* (Plenum Press, New York and London, 1987).
- [28] P. V. Subhash, S. Madhavan, and S. Chaturvedi, *Physics of Plasmas* **13**, 072507 (2006), <https://doi.org/10.1063/1.2222256>.
- [29] J. L. Luxon and L. G. Davis, *Fusion Technology* **8**, 441 (1985), <https://doi.org/10.13182/FST85-A40083>.
- [30] *ITER Technical Basis*, ITER EDA Documentation Series No. 24 (INTERNATIONAL ATOMIC ENERGY AGENCY, Vienna, 2002).
- [31] J. Menard, S. Gerhardt, M. Bell, J. Bialek, A. Brooks, J. Canik, J. Chrzanowski, M. Denault, L. Dudek, D. Gates, N. Gorelenkov, W. Guttenfelder, R. Hatcher, J. Hosea, R. Kaita, S. Kaye, C. Kessel, E. Kolemen, H. Kugel, R. Maingi, M. Mardenfeld, D. Mueller, B. Nelson, C. Neumeyer, M. Ono, E. Perry, R. Ramakrishnan, R. Raman, Y. Ren, S. Sabbagh, M. Smith, V. Soukhanovskii, T. Stevenson, R. Strykowski, D. Stutman, G. Taylor, P. Titus, K. Tresemer, K. Tritz, M. Viola, M. Williams, R. Woolley, H. Yuh, H. Zhang, Y. Zhai, and A. Z. and, *Nuclear Fusion* **52**, 083015 (2012).
- [32] I. Chapman, W. Cooper, J. Graves, M. Gryaznevich, R. Hastie, T. Hender, D. Howell, M.-D. Hua, G. Huysmans, D. Keeling, Y. Liu, H. Meyer, C. Michael, S. Pinches, S. Saarelma, and S. S. and, *Nuclear Fusion* **51**, 073040 (2011).
- [33] J. Boris, Tech. Report NRL Memorandum Report 2167 (Naval Research Laboratory, Washington, DC) (1970).
- [34] P. V. Subhash, S. Madhavan, and S. Chaturvedi, *Physics of Plasmas* **16**, 012701 (2009), <https://doi.org/10.1063/1.3054546>.
- [35] M. R. Halfmoon and D. P. Brennan, *Physics of Plasmas* **24**, 062501 (2017), <https://doi.org/10.1063/1.4984772>.
- [36] D. Chandra, A. Thyagaraja, A. Sen, C. Ham, T. Hender, R. Hastie, J. Connor, P. Kaw, and J. Mendonca, *Nuclear Fusion* **55**, 053016 (2015).
- [37] H. Cai, J. Cao, and D. Li, *Nuclear Fusion* **57**, 056006 (2017).
- [38] O. Tange, *GNU Parallel 2018* (Ole Tange, 2018).